JOURNAL OF MATERIALS SCIENCE 27 (1992) 2211–2217

Design and development of the d.c. plasma reactor for the synthesis of ultrafine powders

C. W. ZHU, G. Y. ZHAO, V. V. S. REVANKAR, V. HLAVACEK
Ceramic and Reaction Engineering Laboratory, Chemical Engineering Department, State University of New York at Buffalo, Buffalo, NY 14260, USA

After analysing different plasma processes, we have designed and developed a 14kW d.c. plasma unit for generating ultrafine powders. Experiments to characterize the torch demonstrated that it is possible to operate the plasma unit over a wide range of conditions without losing its discharge stability. Temperature distribution profiles were determined radially as well as axially in the reaction chamber, and the efficiency of the torch was calculated for a fixed power input. Ultrafine powders of Ta, Mo and W were synthesized, and size and size distribution obtained. The particle size was found to be 0.03–0.1 μm, with a perfect spherical shape. The analysis of the samples is discussed.

1. Introduction

Advanced ceramics and refractory materials have recently received considerable attention due to their high strength, hardness, and resistance to corrosion and to high temperatures. The quality of those materials is to a large extent controlled by the characteristics of the starting powders used. General requirements are high purity, desired particle size and size distribution, shape and morphology, fraction of crystalline phase and easy sinterabilty. However, different processes are available, including thermal plasma, with its clean electrical energy, high efficiency, perfect controllability, inherent high temperature (10^4 K), steep temperature gradient (10^6 K m^{-1}), fast quench rate (10^6 K s^{-1}). Materials with highly excited states (such as dissociated atoms, ions, radicals, activated atoms or molecules) offer a unique technological advantage for the production of high-technology materials. Ultrapure and ultrafine powders of ceramics and refractory metals can be produced using plasma processes [1, 2]. Many plasma chemical vapour deposition (CVD) processes have been studied to produce ultrafine ceramic powders using RF plasma [3, 4] and d.c. plasma [5, 6].

D.c. plasma is mostly operated at atmospheric pressure when a high-energy transfer is required, especially when handling the solid reactants. However, r.f. plasma is an electrodeless discharge, therefore electrode contamination can be avoided, even with low-pressure operation. If these two operations are compared, d.c. plasma stands alone with its high power (10 MW), high efficiency, cheaper capital equipment cost, and high material processing capability at atmospheric pressure. A variety of compounds and refractory materials can be synthesized in the d.c. plasma, as described elsewhere [7].

The aim of this research is to design and develop a 14kW d.c. plasma system for the preparation of ultrafine powders. Initial experiments were conducted to generate powders of Ta, Mo and W by reduction of corresponding chlorides. Efforts were made to characterize the torch and its thermal efficiency. The temperature distribution profiles in the reactor were located which will determine the characteristics of the powders. Experiments were also conducted to demonstrate stable operating conditions without losing thermal efficiency. The generated Ta, Mo and W powders were analysed for their purity, particle size and shape, and other characteristics.

2. Experimental procedure

2.1. Set-up

The design and fabrication of the d.c. plasma unit is a tedious job and should be handled very carefully. The experimental system used in our operation is shown in Fig. 1, and can be divided into five main parts.

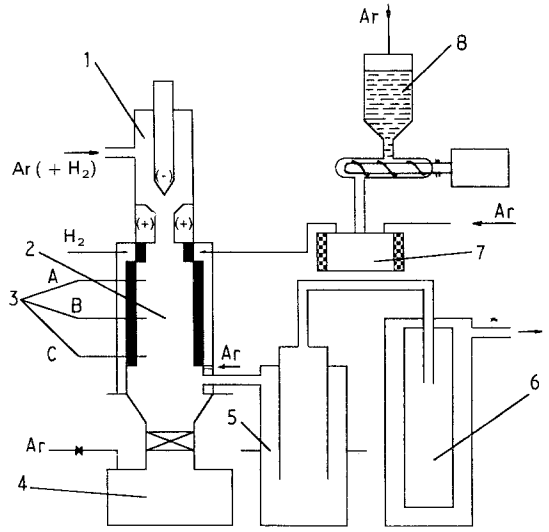

Figure 1 Experimental layout of d.c. plasma system. 1: plasma torch; 2: reactor; 3: thermocouple; 4: collector; 5: cyclone separator; 6: bag filter; 7: evaporator; 8: feeding system.

2.1.1. Plasma torch

Several components were identified with the d.c. plasma torch: cathode, anode, cooling water jacket, plasma gas and power input systems. The cathode was fabricated using standard design with a 60° conical tip made up of thoriated tungsten (tungsten and zirconium alloyed tungsten were kept as standbys). The anode was made up of copper, and had a convergent throat shape with a nozzle 6 mm in diameter. The length of the anode can be changed very easily according to requirements. (This may also be called an arc plasma torch, where plasma stabilization takes place by eddy gases.) The plasma gases were injected into the system tangentially and passed through the gap between the cathode and the anode created by the special swirling channel (the large swirling velocity is necessary for a stable plasma arc). These gases were simultaneously passed through four screens mounted in series in front of the anode to reduce the turbulence. The first three screens were of 250 mesh size, and the last 100 mesh size. The distance of the gap, L, between the cathode and the anode was adjustable by a screwing arrangement, which is important to the operating condition of the torch. An independent cooling system was provided for both cathode and anode. The power supply was connected to cathode and anode by the cooling water output lines; the anode was electrically grounded.

2.1.2. Reactor

The reactor assembly consisted of a feeding arrangement just next to the torch exit, a reaction chamber, quenching section and powder collector. The feeding section was made up of a stainless steel material with a chilled water circulation jacket. Two observation windows, 10 mm in diameter of quartz, were mounted radially opposite to measure and observe the plasma characteristics. Four feeding ports (1.5 mm inside diameter) were kept radially on this part, equidistant from each other, to feed the gaseous or liquid reactants. The reaction chamber, which was connected to the feeding chamber, consisted of a high-quality graphite tube (50 mm inside diameter and 250 mm in length), enclosed in a concentric stainless steel jacket with cooled water circulating around it. Three thermocouple holes were provided to measure the temperature profile along the axis of the reaction chamber. The first was located on section A which was 62 mm from the torch exit section (i.e. inlet of the reactor); the second was located on section B; and the third on section C, which were 130 mm and 260 mm from section A, respectively. The quenching chamber which followed the reaction chamber was also made up of stainless steel materials with four quenching gas ports (6 mm inside diameter) mounted radially on it. The first powder collector was located on the bottom of the reactor: it was also made of stainless steel. Exit gases from the reactor passed through the cyclone, bag filters and scrubber.

2.1.3. Feeding system

The main parts of the feeding system were a variable speed motor, a screw feeder and an evaporator. The feed rate of the solid reactants to the evaporation chamber could be changed by means of the variable speed of the d.c. motor. The feeding capacity could be varied from 0.1 to 20 g min^{-1}. The vapour of the evaporated powders was fed to the plasma tail by a carrier gas. The total system was heated to the required temperature by means of a heating coil, which was very important to avoid clogging the feed lines. The evaporator chamber was made of super graphite with 50 mm inside diameter and 120 mm length. The total heating power of the evaporator was 1.5 kW.

2.1.4. Collector

Other than the collector at the reactor bottom end, we connected the cyclone separator and bag filters in series. Bag filters can retain final submicrometre powders, as demonstrated by our experiment. The general scrubber was attached to the vent gases.

2.1.5. Power supply

The maximum open circuit voltage was 59.4 V, and the permissible maximum current 230 amperes in the continuous operation. The power supply had a h.f. source with a frequency of 1 MHz and a voltage of 3000 V, which could be used to start the discharge of the d.c. torch. The power supply current could maintain any constant value in the permissible range, according to the adjustment. Other factors were not influential. Thus the load line had an infinite slope, as shown in Fig. 2.

2.2. Plasma torch characteristics and temperature profile in the reactor

Before starting the measurements, we calibrated the entire system from ammeters, voltmeters, flow meters and thermocouple to temperature indicators. An argon plasma jet, at various rates and at atmospheric pressure, was employed as a thermal plasma flow. The plasma arc was generated by an arc discharge between

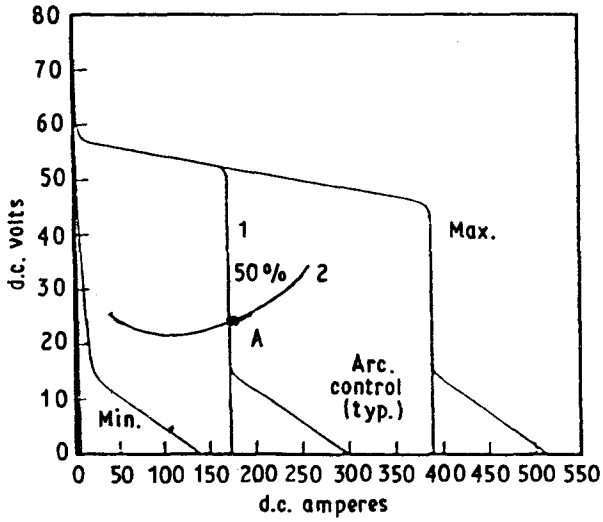

Figure 2 Current and voltage characteristics of power supply. 1: load line. 2: arc characteristic.

TABLE I Experimental data

Starting materials	Feeding rate ($g\,min^{-1}$)	Ar plasma flow rate ($L\,min^{-1}$)	Ar carrier flow rate ($L\,min^{-1}$)	Hydrogen flow rate ($mL\,min^{-1}$)	Reaction temperature (°C)
$TaCl_5$	2	35	10	1360	900
$MoCl_5$	2	35	10	2241	800
WCl_6	2	35	10	1253	800

a copper nozzle anode and a thoriated tungsten cathode. The measurements were then carried out for the current–voltage characteristics of the torch for various plasma gas flows. The plasma tail temperature field in the reaction section of the reactor was measured using a special thermocouple located in the A, B and C sections of the reactor. Thermocouples could be moved freely along the radial direction, and temperature was measured at different points under steady-state operating conditions. This gave temperature values for both radial and axial directions in the reactor.

The torch thermal efficiency as a function of plasma gas-flow rate was determined. The overall thermal conversion efficiency is defined as the ratio of the energy carried by the plasma gas to the input electrical energy, and is expressed in the form

$$\eta = (V_a I_a - M_w C_p T)/V_a I_a \quad (1)$$

where V_a is the arc voltage, I_a is the arc current and M_w, C_p and T are the mass flow rate, specific heat and the temperature difference in the inlet and outlet cooling-water temperature of the torch electrodes, respectively.

2.3. Synthesis of ultrafine powders

As a first step, we considered the following systems for generating ultrafine powders of Ta, Mo and W, where the respective chlorides were reduced by hydrogen.

$$2TaCl_5 + 5H_2 = 2Ta + 10HCl \quad (2)$$

$$2MoCl_5 + 5H_2 = 2Mo + 10HCl \quad (3)$$

$$WCl_6 + 3H_2 = W + 6HCl \quad (4)$$

The chlorides were fed through the screw feeder at a selected standard feed rate to the evaporator, which was heated to 800 °C. The vapour of evaporated materials was carried away by the Ar carrier gas to the reaction chamber (into the plasma tail) where they were reduced, and the generated ultrafine powders were collected at various sections. At the beginning, the main problem in this operation was the plugging of the lines, especially in the section where the feed line passed through the water-cooling steel jacket of the reactor. To overcome this problem, we heated the entire transport lines and entrance section of the reactor.

The main plasma-forming gas was the mixture of Ar and H_2. Part of the hydrogen bypassed the torch and entered the reactor directly, for the reduction process to produce the ultrafine nuclei. The working gas temperature in the reactor could be adjusted by changing the supply current or the quantity of Ar and H_2 flow rates in the plasma-forming gases. The final operating conditions are summarized in Table I.

4. Results and discussion

Fig. 3 plots arc voltage against current, with the distance of the gap between cathode and anode (L) at 0.25 cm, and at different plasma argon gas-flow rates. These plots show a similar pattern for all three flow rates studied. The relation can be represented, as given by Pfender [8] and Ayrton [9]

$$V_a = a + bL + [(c + dL)/I_a] \quad (5)$$

and [8, 10]

$$V_a = 4.3 I_a^{0.25} L^{0.3} \quad (6)$$

where I_a is in amperes, L is in centimetres, and the constants a, b, c, and d must be determined from the experiment. Equation 5 applies only to arcs with falling characteristics, as the current parameter is in the denominator. Equation 6 applies only to a free-burning high intensity argon arc with a water-cooled anode for the parameter range $200 \leq I \leq 2300$ A and $0.5 \leq L \leq 3.15$ cm. This phenomenon can be explained using the above equations. The characteristic falling trend was a result of increasing arc conductance with increasing current, which may be either by an increase in electrical conductivity, or arc diameter, or both. In a high-intensity arc, this general trend may be overbalanced by disproportionally high losses from the arc, to which the arc responds with an increase in field strength. In general, no prediction about the characteristics of arcs can be made because the external conditions such as stabilizing walls, magnetic or gas dynamic fields, etc., may reverse the trends. The interception point of the arc characteristics and the load line, for example point A on Fig. 2, determines the operating conditions of the torch if the Kaufman stability criterion is satisfied. However, this criterion is satisfied at any one interception point where the load line has an infinite slope. The rising characteristic further improves the arc discharge stability. The dis-

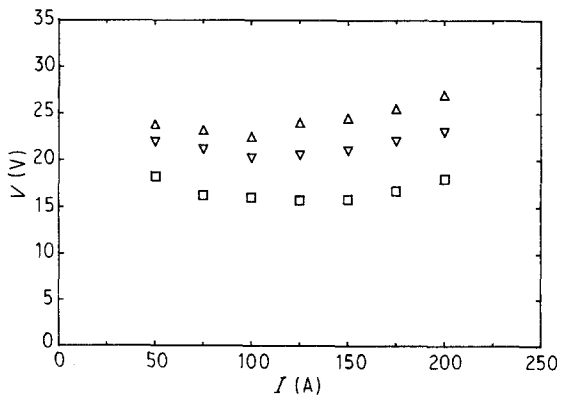

Figure 3 Current and voltage characteristics of plasma arc. △, 3; ▽, 2; □, 1 $m^3\,h^{-1}$. Gap between cathode and anode = 2.5 mm.

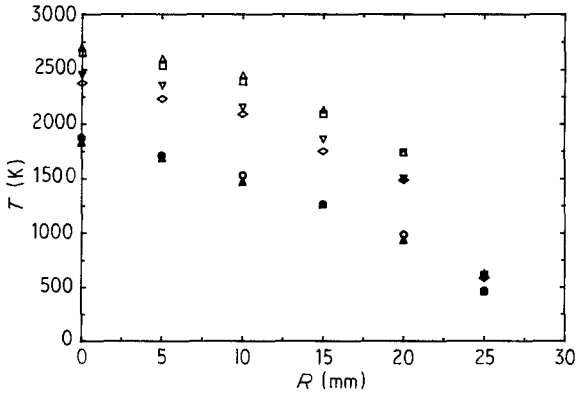

Figure 4 Radial temperature distribution in section A of the reactor. △, 2; □, 3 $m^3 h^{-1}$, 10 kW. ▽, 2; ◇, 3 $m^3 h^{-1}$, 7 kW. ○, 2; ▲, 3 $m^3 h^{-1}$, 4 kW.

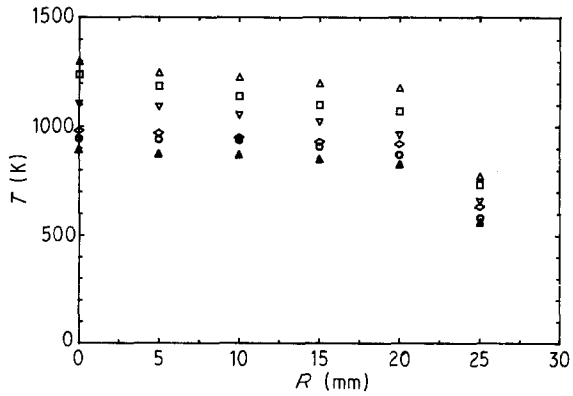

Figure 6 Radial temperature distribution in section C of the reactor. △, 2; □, 3 $m^3 h^{-1}$, 10 kW. ▽, 2; ◇, 3 $m^3 h^{-1}$, 7 kW. ○, 2; ▲, 3 $m^3 h^{-1}$, 4 kW.

tance of the gap L depends on power requirements and flow rate. But we did not observe much change in this characteristic when we slightly changed the gap.

Fig. 4 is the radial temperature distribution profile for section A. It can be seen that the temperature is highest at the centre and then decreases almost linearly. At lower power, the change in the flow rate hardly affects the distribution profile, whereas this is noticeable at the high-power region. At a particular power, there was a decrease in temperature with flow rate. The highest temperature obtained was around 2750 K, at an input power of 10 kW. The wall temperature was hardly affected by any of these variations.

Figs 5 and 6 show radial temperature distribution profiles for sections B and C, respectively. These showed similar patterns to that in section A, but at lower temperatures. At an input power of 10 kW, the highest temperature in section B was 2050 K, and in section C was around 1300 K. Again, wall temperature was nearly unaffected by the variables. Fig. 7 shows the axial temperature distribution profile at the centre of the reactor starting from section A. Here the temperature also decreased linearly along the axis and the maximum temperature depended on the operating conditions such as gas-flow rates and input power. The temperature did not vary much in the central zone of the reactor, which is very important to achieve uniform particles.

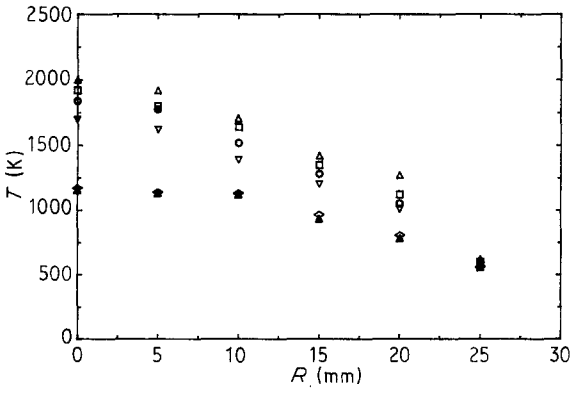

Figure 5 Radial temperature distribution in section B of the reactor. △, 2; □, 3 $m^3 h^{-1}$, 10 kW. ○, 2; ▽, 3 $m^3 h^{-1}$, 7 kW. ◇, 2; ▲, 3 $m^3 h^{-1}$, 4 kW.

The torch thermal efficiency is shown in Fig. 8, where thermal efficiency is plotted against flow rate. The thermal efficiency increased with increasing gas-flow rate before stabilizing. The thermal efficiency was calculated for the total input power of 7 kW in this particular case.

The reduction of $TaCl_5$, $MoCl_5$ and WCl_6, as shown in Equations 2–4, was carried out in the d.c. plasma reactor to determine the powder characteristics. The above mechanism is the simple form of a complex reaction occurring in the reduction process. The $TaCl_5$ (m.pt 220 °C, b.pt 233–239 °C), $MoCl_5$ (m.pt

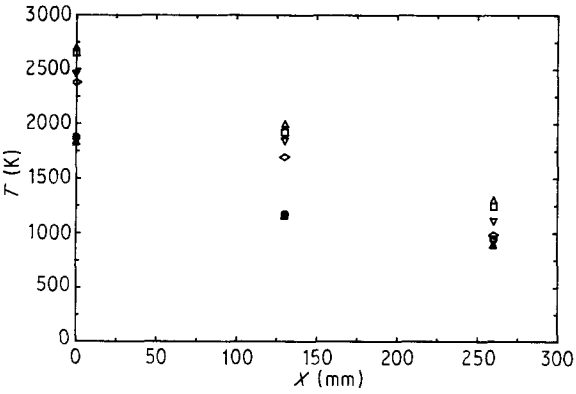

Figure 7 Axial temperature distribution in the central line of the reactor. △, 2; □, 3 $m^3 h^{-1}$, 10 kW. ▽, 2; ◇, 3 $m^3 h^{-1}$, 7 kW. ○, 2; ▲, 3 $m^3 h^{-1}$, 4 kW.

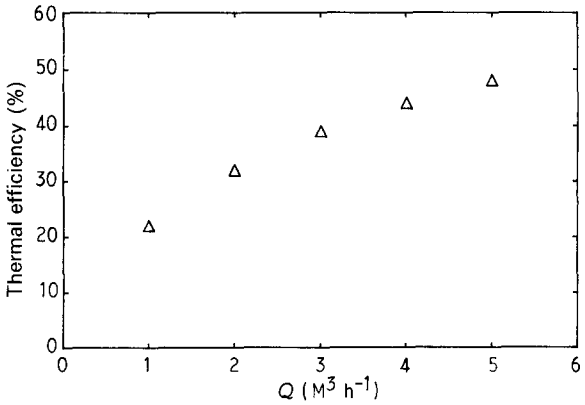

Figure 8 Thermal efficiency plot for the torch. $P = 7$ kW.

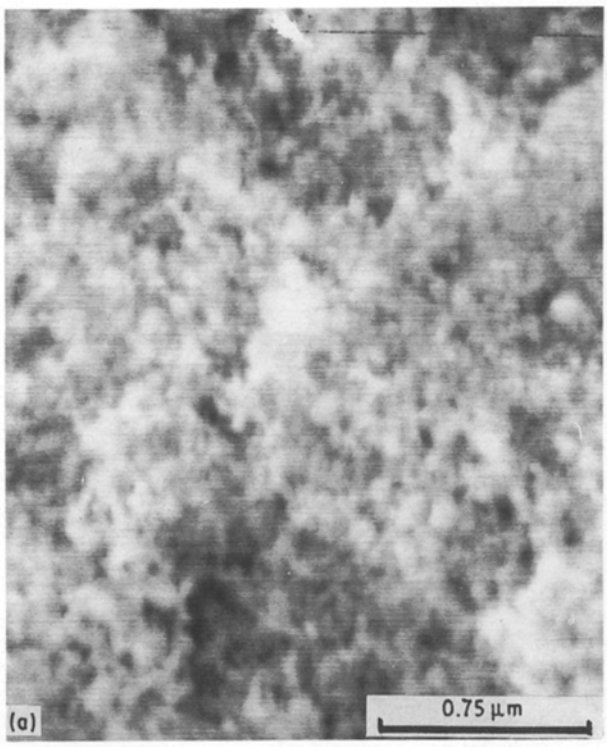

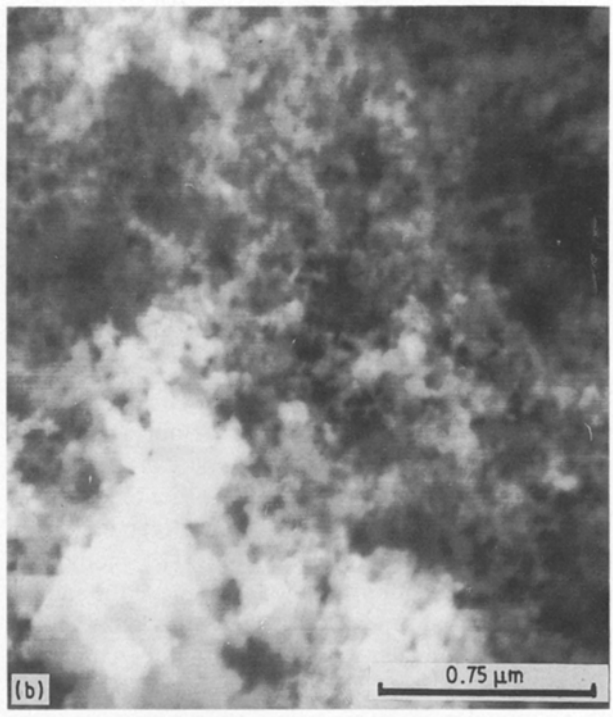

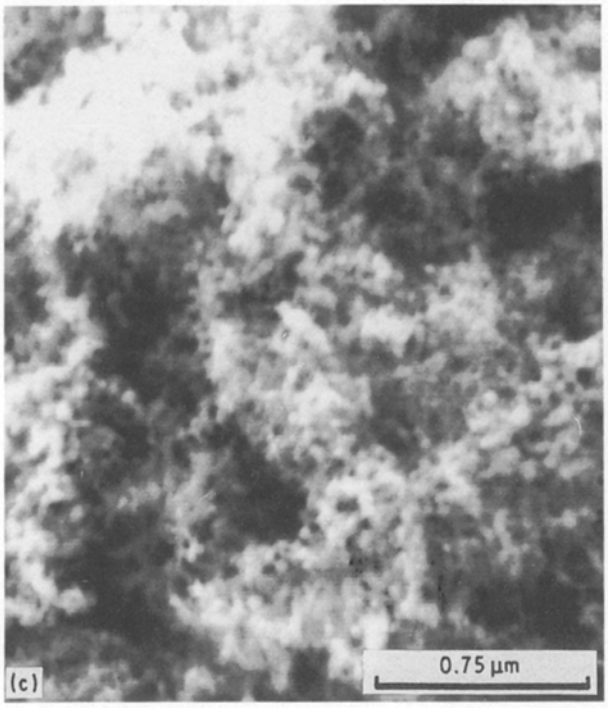

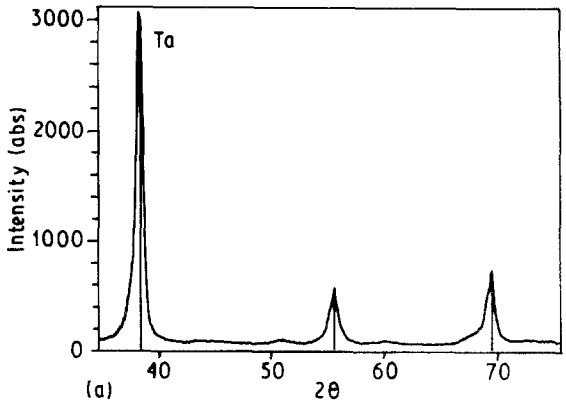

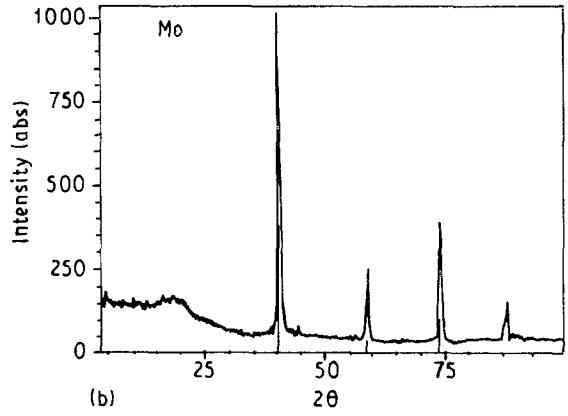

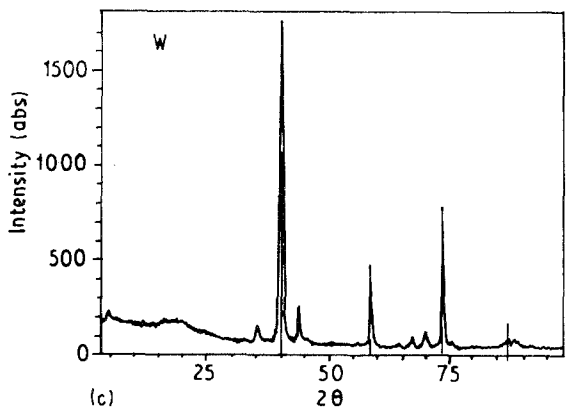

Figure 9 Scanning electron micrographs of (a) Ta; (b) Mo; and (c) W powders.

194 °C, b.pt 264 °C) and WCl_6 (m.pt 275 °C, b.pt 347 °C) are believed to be dissociated into several subchlorides, the proportion of each being determined by the temperature to which the reactants were heated. These subchlorides finally react with hydrogen to produce Ta, Mo, and W ultrafine powders. The molar ratio of hydrogen (H_2) to metal chlorides is very important to get nonpyrophoric Ta, Mo and W powders. We obtained these powders at the H_2/metal chloride molar ratio between 5 and 12.

It is important that the system should be free of moisture and oxygen, as the powders generated are ultrafine and highly reactive. The possible sources of contamination are (i) the starting reactant, as it is or as an oxychloride; (ii) leakage in any part of the system; (iii) on exposure to the atmosphere (either oxidation or pyropheric nature of the product); and (iv) materials of the system and electrode burnout. The method of collection is also important, for example, if the sample is collected in an open atmosphere, this gives 8% of oxygen in the powder within a few minutes, compared to less than 1% in N_2 or Ar atmosphere. The analysis of Ta powder is given below in p.p.m., using the industrial grade $TaCl_5$ and pre-purified grade Ar and H_2 as starting materials.

Al[20], B[< 6], Be[< 6], Ca[< 6], Cr[< 200], Cu [200], Fe[600], Mg[< 6], Mo[200], Mn[20], Na[< 6], Ni[200], Pb[< 20], Si[200], Sn[< 6], Ti[< 6]

It appears that there is more Fe in the sample which can be decreased by improving the operating conditions and cleaning the reaction system. The size and the size distribution of particles are very important parameters for sintering. The SEMs and image analysis in Fig. 9 show that the average particle size is around 0.03–0.05 μm with the smallest particles being around 0.01 μm. All the particles appear to be below 0.1 μm. Particles are perfectly spherical or cubic, with spherical being the predominant shape. However, the traditional size distribution measurement (centrifugal) showed a much higher size distribution, as shown in Fig. 10. This may be due to agglomeration of the particles which creates these errors. In this method, the average particle size of Ta, Mo and W is 0.69, 0.69 and 0.74 μm, respectively. Whatever the reason, in both cases the particle size appears to be very small, and the distribution is very narrow. This depends on many factors, from partial pressure of the reactants, reaction temperature, residence time, and quench rates, to mixing of the reaction materials. Any adjustment of these parameters may alter the size and the size distribution of the powders. The bulk density of the powders of Ta, Mo and W is around 0.355, 0.347 and 0.350g cm^{-3}, respectively. The surface areas are around 14.000, 12.528 and 25.528 $m^2 g^{-1}$, respectively.

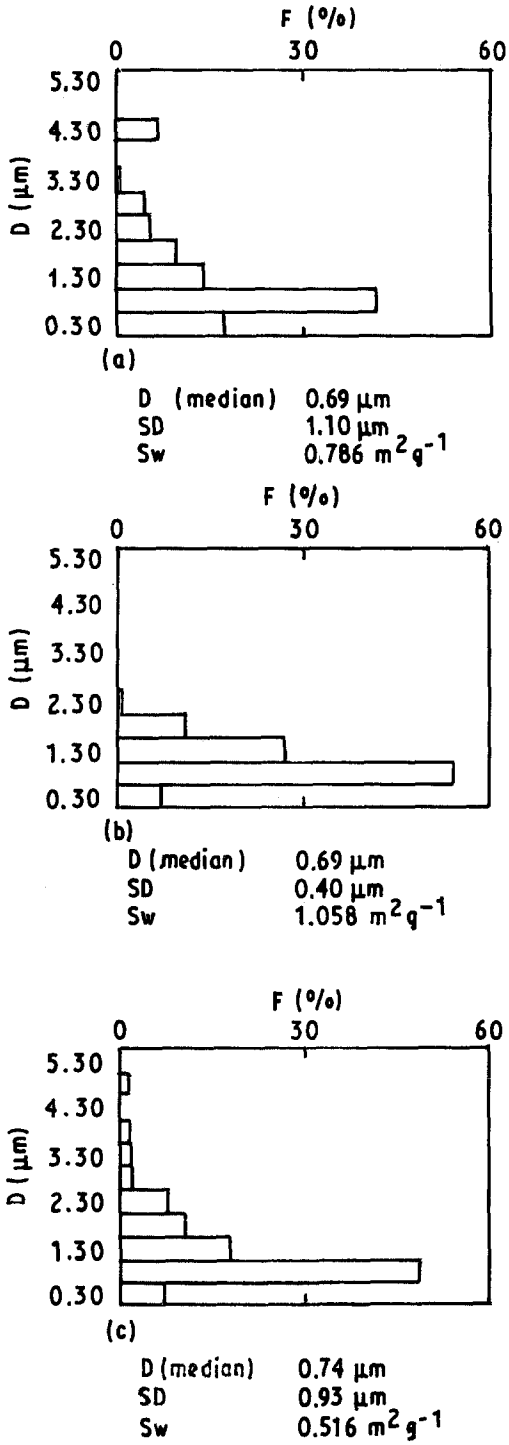

Figure 10 Size distribution plots for (a) Ta; (b) Mo; and (c) W powders. D, particle diameter; F, frequency distribution; D (median), average particle diameter; SD, standard deviation and SW, surface area.

5. Conclusions

A 14 kW d.c. plasma unit has been successfully designed and developed to synthesize ultrafine powders by a chemical vapour reaction method. Ultrafine refractory metal powders of 0.03–0.1 μm with a narrow size distribution were produced and studied. The electrical characteristics of the torch and the temperature field in the reactor were investigated. This work can be used for possible scaling up of the d.c. plasma and CVD reactors, and for many other applications.

References

1. P. FAUCHAIS, E. BOUDRIN, J. F. COUDERT and R. McPHERSON, "High Pressure Plasmas and their Application to Ceramic Technology: Topics in Current Chemistry, edited by F. L. Boschloe (Springer, New York, 1983) **107**, p. 62.

2. C. W. ZHU *Adv. Mech.* **16** (1986) 281.
3. K. AKASHI, "Progress in Thermal Plasmas Deposition of Alloys and Ceramics Fine Particles" (ISPC-7 Eindhoven, 1985) 13.
4. C. W. ZHU, and J. P. YANG, *J. Chem. Ind. Engng* **39** (1988) 180.
5. T. N. MEYER, A. J. BECKER, J. E. EDD, F. N. SMITH and J. LIU, "Plasma Synthesis of Ceramic Powders" (ISPC-8, Tokyo, 1987) 2006.
6. R. M. YOUNG, Y. CHANG, LECERF and E. PFENDER, "Plasma Synthesis of Ceramic Powders" (ISPC-8, Tokyo, 1987) 2028.
7. E. PFENDER, "Thermal Plasma Processing in the Nineties" (ISPC-8, Tokyo, 1987) 2.
8. E. PFENDER, "Electric Arcs and Arc Gas Heaters, from the Gaseous Electronics", edited by Merle N. Hirsh and H. J. Oskam (Academic, New York, 1978) p. 346.
9. H. AYRTON, "The Electric Arc (The Electrician Co., London, 1902).
10. R. C. EBERHART and R. A. SEBAN, *Int. J. Heat Mass Transfer* **9** (1966) 939.

Received 7 January
and accepted 7 June 1991